

Switching Control of Latex Balloon Expansion by using Switching Valve mediated with the Coanda Effect

Keita Kaneko

Keio University Faculty of Science and Technology Graduate School of Science and Technology: Keio Gijuku Daigaku Rikogakubu Daigakuin Rikogaku Kenkyuka

Kenjiro Takemura (✉ takemura@mech.keio.ac.jp)

Keio University Faculty of Science and Technology Graduate School of Science and Technology: Keio Gijuku Daigaku Rikogakubu Daigakuin Rikogaku Kenkyuka <https://orcid.org/0000-0002-0298-5558>

Research Article

Keywords: Soft robot, Fluidics, Coanda effect

Posted Date: January 10th, 2022

DOI: <https://doi.org/10.21203/rs.3.rs-1203430/v1>

License:   This work is licensed under a Creative Commons Attribution 4.0 International License.

[Read Full License](#)

1 **Switching Control of Latex Balloon Expansion by using Switching Valve mediated** 2 **with the Coanda Effect**

3 Kaneko Keita¹ and Takemura Kenjiro^{2*}

4 *Correspondence: takemura@keio.mech.ac.jp

5 ¹Graduate School of Science and Technology, Keio University, 3-14-1 Hiyoshi Kohoku-ku, Yokohama, Kanagawa 223-
6 8522, Japan.

7 ²Department of Mechanical Engineering, Keio University, 3-14-1 Hiyoshi Kohoku-ku, Yokohama, Kanagawa 223-
8 8522, Japan.

9 **Abstract** Soft robots have advantages in terms of safety, softness, and compliance compared to traditional
10 robotic systems. However, fluid-driven soft actuators, often employed in soft robots, require a
11 corresponding number of bulky pressure supplies/valves to drive. Here, we consider a valve that can control
12 the flow without mechanical moving parts for simplifying the driving system of soft actuators. We
13 developed a system comprising a pump, a switching valve, and two latex balloons to demonstrate the
14 feasibility of introducing a fluid valve into soft robotics. As the valve, which makes use of the Coanda
15 effect, can switch the flow between two outlets when the pressure difference between the outlets is 3 kPa,
16 we employed a latex balloon connected to each outlet. The system can control the expansion of each balloon
17 by switching the flow from the pump. The experimental results proved that the system could actuate each
18 balloon.

19 **Keywords** Soft robot · Fluidics · Coanda effect

20 **Introduction**

21 In recent years, there has been a growing demand for robots that can operate in human environments and
22 be used for nursing, entertainment, customer service, etc. [1]. Such robots are expected to be safe to reduce
23 possible physical harm when they come in contact with humans, flexible enough to behave similar to living
24 organisms, and compliant enough to cope with unexpected situations and environments [2–4]. For these
25 reasons, soft robots, in which the structure and actuators are flexible, have attracted wide attention [5].
26 Soft robots are often constructed and actuated using fluid-driven flexible rubber actuators [6]. Thus, a
27 critical issue arises. When developing a soft robot, the mass and volume of the entire system increases as
28 multiple pressure sources/valves are required based on the number of degrees of freedom of motion required

29 by the robot. A large number of studies have been reported on the application of pneumatic soft robots,
30 where multiple motions were generated using a single compressor and several valves, suggesting the
31 possibility of increasing the degrees of freedom with mechanically driven pneumatic components located
32 outside a robot [7–9]. Compared to pneumatically driven soft robots, hydraulic systems for soft robotics
33 have not yet been extensively explored. Previously reported hydraulic soft robots employ rigid and bulky
34 fluid control components [10, 11].

35 Considering the abovementioned background, we focused on using a valve, as one of the most important
36 elements of *fluidics*, to simplify the entire system. The idea is to realize a multi-degree-of-freedom motion
37 by appropriately switching the pressure flow, generated by a pressure source, using a simple switching
38 valve. To demonstrate this concept, the current study aims to realize a fluid-driven system that can
39 selectively expand balloons using a simple switching valve.

40 **Materials and Methods**

41 **Concept**

42 Fig. 1 shows a schematic of the proposed drive system, capable of selectively expanding each of the two
43 balloons. The proposed drive system comprises a pump (not shown in the figure), a fluidic switching valve,
44 balloons, and throttle valves. The fluidic switching valve switches the direction of the main flow, discharged
45 from the pump into one outlet, using the Coanda effect [12] induced by the control flow. The throttle valve
46 increases the gauge pressure of the balloon connected to the outlets; therefore, the gauge pressure of the
47 target outlet of the switching valve is higher than that of the other. The difference in gauge pressure, due to
48 the difference in flow rate, creates a difference in the balloon deformation. Switching the control flow
49 causes the target outlet to switch, deflates the inflated balloon, and inflates the non-inflated balloon. This
50 achieves a selective drive of multiple balloons with relatively simple configurations, thus, downsizing the
51 entire system. It can be observed that there is a need for an additional control system for appropriately
52 generating control flows 1 and 2. The control system may be implemented in a fluid circuit, for example,
53 by feeding the outlet flow from the throttle valves to the control flow inlets to achieve a replicating motion
54 of balloons. Therefore, this study simply shows that the Coanda effect employed in a simple fluidic valve
55 may contribute to the selective drive of each balloon.

56 **Fluidic Switching Valve**

57 Figs. 2a and 2b show an overview of the fluidic switching valve, which is an important element in *fluidics*.
58 *Fluidics* aims to realize logic circuits, such as electronic circuits, using fluid flow. To achieve this, many
59 fluidic logic elements employ the Coanda effect, in which fluid flow along a channel adheres to a channel
60 wall [12]. We used this digital switching function for driving soft actuators. A fluidic switching valve can
61 select the discharge outlet of the flow from the pump (main flow) by inputting a small amount of flow from
62 the side (control flow). In other words, the main flow can be directed into outlet 1 by inputting control flow
63 1, and the same is true for outlet 2 (see Fig. 2).

64 Fig. 2c shows a schematic of the Coanda effect observed in the fluidic switching valve. The flow velocity
65 distribution is mapped on the model, which was calculated using the k- ϵ turbulence model for a low
66 Reynolds number. Note that the condition for the numerical simulation is as follows: the main flow velocity
67 is 0.7 m/s; the control flow 1 velocity is 0.04 m/s; the control flow 2 velocity is 0 m/s. As shown in Figs.
68 2a, 2b, and 2c, the difference in the discharge flow rate between the outlets was created by the negative
69 pressure in a vortex created by the Coanda effect at the flow divergence area. The Coanda effect refers to
70 the fluid property in which the jet flows along a curved surface and is less prone to flow separation than a
71 uniform flow [13]. For this reason, in the fluidic switching valve, shown in Fig. 2c, the main flow adheres
72 to the wall on either side of the direction of the flow in the separation area. The valve can select the wall
73 that the main flow should adhere to by introducing a control flow perpendicular to the main flow at the flow
74 divergence area, which means that the valve can switch the discharge outlet.

75 Figs. 2d and 2e show the dimensions and an actual view of the developed fluidic switching valve. The
76 diameters of the main flow inlet, control flow inlet, and outlet were 13 mm, 3 mm, and 3 mm, respectively.
77 The cross-section of an orifice, where the main flow and control flow collide, was a rectangle with a width
78 of 2 mm and a thickness of 3 mm. Water was employed as the working fluid.

79 **Throttle Valve**

80 Figs. 2f, 2g, and 2h show schematics of the throttle valve and its model. The throttle valve intentionally
81 creates pressure loss according to the flow rate through the valve. The pressure loss, ΔP , can be calculated
82 using the loss coefficients, K , as

$$83 \quad \Delta P = K \frac{\rho V^2}{2}, \quad (1)$$

84 where ρ is the density, and V is the velocity. Therefore, the pressure loss is proportional to the square of the

85 velocity. In addition, the loss function K can be considered as that for sudden contraction, K_{SC} , and that for
 86 sudden expansion, K_{SE} . The theoretical loss coefficient for a sudden expansion is expressed as

$$87 \quad K_{SE} = \left(1 - \frac{d^2}{D^2}\right)^2, \quad (2)$$

88 where d is the diameter of the narrow area of the tube, and D is the diameter of the wide area of the tube.
 89 In addition, the loss coefficient for a sudden contraction fits the empirical formula as

$$90 \quad K_{SC} \approx 0.42 \left(1 - \frac{d^2}{D^2}\right) \quad (3)$$

91 up to the value $d/D = 0.76$, above which it merges into Equation (2). Therefore, the total pressure loss,
 92 which equals the inner pressure of the balloon, can be written as:

$$93 \quad \Delta P_{total} = K_{SC} \frac{\rho V_D^2}{2} + K_{SE} \frac{\rho V_d^2}{2} = \frac{\rho V_D^2}{2} \left[0.42 \left(1 - \frac{d^2}{D^2}\right) + \frac{D^2}{d^2} \left(1 - \frac{d^2}{D^2}\right)^2 \right] \quad (4)$$

$$94 \quad \because V_d \frac{1}{4} \pi d^2 = V_D \frac{1}{4} \pi D^2.$$

95 Note that these equations can be applied only to sudden extraction (contraction). However, we employed a
 96 roller clamp (KT-6, Cole-Parmer LLC, USA) as the throttle valve, to obtain well-rounded entrance and exit
 97 of the throttle valve. Therefore, the actual loss coefficient for contraction is considered negligible ($K =$
 98 0.05), and that for extraction is considered to be lower than that for sudden expansion [14].

99 **Balloon**

100 As shown in Figs. 2a and 2b, directing the main flow to outlet 1 (2) creates a difference in the discharge
 101 flow rate between the outlets. This flow rate difference causes the gauge pressure of the balloon to be
 102 connected to the outlets owing to the throttle valve (cf. Fig. 1 and Fig. 2c). Therefore, the differential
 103 deformation in the balloon is achieved by the pressure difference, ΔP , which depends on the flow rate
 104 difference between the outlets of the fluidic valve. However, as shown in Fig. 2c, the flow rate difference
 105 produced by the fluidic switching valve depends on the Coanda effect at the flow divergence area. Therefore,
 106 the fluidic switching valve cannot maintain the flow rate difference if the pressure applied to the target
 107 outlet is large.

108 To ensure sufficient deformation difference between the balloons, we employed a latex balloon. Figs. 3a
 109 and 3b show schematic PV diagrams of a balloon with a) linear and b) nonlinear relation between the

110 internal pressure and volume. In the case of a balloon with a linear PV diagram (a), ΔP must be large to
111 produce a sufficient deformation difference. On the other hand, a balloon with a peak in the PV diagram
112 (b) deforms slightly up to a threshold pressure and deforms significantly at the threshold pressure and
113 beyond. In other words, it is possible to produce a sufficient deformation difference between the balloons
114 with a peak in their PV diagram when the gauge pressure difference, ΔP , exceeds the threshold value.
115 Fig. 3c shows the PV diagram of the latex balloon employed in this study. The PV diagram was measured
116 by injecting water into the balloon with syringes (SS-50ESZ and SS-10ESZ, Terumo Corporation, Japan).
117 The balloon was injected with water in a 0.2 mL step up to 12 mL and later, in a 1 mL step. The internal
118 pressure of the balloon was measured with a pressure gauge (GC-31-174, Nagano Keiki Co., Ltd., Japan)
119 at each step. The peak internal pressure on the PV diagram was 8 kPa when the volume of the balloon was
120 approximately 5 mL. Beyond this, the internal pressure decreased as the volume increased. It was confirmed
121 that the balloon deformed significantly at a threshold value of approximately 8 kPa and higher.

122 **Fabrication of Components**

123 Fig. 4 shows the developed system. The system consisted of a positive displacement pump (V-15, Iwaki
124 Corporation, Japan), a fluidic switching valve developed in this study, syringes (SS-50ESZ, Terumo
125 Corporation, Japan), tubing connectors (TPX Tubing Connector 3549, Sanwaplatec Co., Ltd., Japan),
126 balloons (polka dot balloon, Tiger Rubber Co., Ltd., Japan), and throttle valves. The balloons were
127 connected to the fluidic switching valve via tubing connector. Water was as the working fluid in the
128 subsequent experiments.

129 **Experimental Results and Discussion**

130 **Switching characteristics**

131 Fig. 5a shows the experimental setup for switching characterization. The positive displacement pump was
132 connected to the main flow inlet of the fluidic switching valve, and the control flow inlet 2 was closed. The
133 syringe was connected to control flow inlet 1 to direct the main flow to outlet channel 1. A flowmeter (SEN-
134 HZ06K, Uxcell, China) was connected to each outlet to measure the flow rate along each outlet channel.
135 The flow rate of the main flow was varied from 1.2 to 23.3 mL/s in 20 equal intervals, and the flow rate of
136 control flow 1 was set to 7.8 mL/s. In addition, the cross-section ratio of the throttle valve, connected to
137 each outlet, was varied from 59% to 100% (fully closed) in five intervals. Fig. 5b shows the flow rate

138 difference between the outlet 1 and outlet 2 ($Q_{out\ 1} - Q_{out\ 2}$). The volumetric flow rate discharged from the
139 outlet 1 was about 0.25 mL/s higher than that from the outlet 2 in almost all conditions.

140 **Balloons deformation**

141 The deformation of the balloon was visually recorded with different combinations of parameters, main flow
142 rate and cross-section ratio of the throttle valve. The flow rate of main flow was varied from 1.2 to 23.3
143 mL/s in 20 equal intervals. In addition, the cross-section ratio of the throttle valve ranged from 59% to
144 100% in 5 intervals. The flow rate of the control flow 1 was set to 7.8 mL/s, and the control flow 2 was
145 closed. The main flow and control flow 1 were introduced at $t = 0$ s, and after a sufficient time (7.6 s, time
146 at which the syringe was empty), the flow stopped.

147 Figs. 6a and 6b show the defined status of the balloons and a summary of the experimental results. We
148 defined the behavior of the balloon as follows: (a) both balloons are always inflated with or without control
149 flow, (b) one of the balloons inflates but does not deflate when the control flow is stopped; (c) one of the
150 balloon inflates at will and deflates when the control flow is stopped (desired behavior), (d) one or both
151 balloons do not inflate much, and (e) neither of the balloons inflate at all. Fig. 6c shows the deformation of
152 the balloons at a cross-section ratio of 59% and a flow rate of 9.5 mL/s for the main flow. The time required
153 for the blue balloon to deflect under this condition was 4 s and that for the yellow balloon was 6 s. Fig. 6d
154 shows the deformation of the balloon at a cross-section ratio of 59% and a flow rate 10.8 mL/s for the main
155 flow. Under this condition, the time required for the blue balloon to deflect was 12 s and that for the yellow
156 balloon was 83 s. (i) and (iv) in Figs. 6c and 6d show the initial state of the balloons at t or $t' = 0$ s. Note
157 that t and t' represent the time for introducing the control flows 1 and 2, respectively. When the water in
158 the syringe is fully injected at t ($t' = 7.6$ s), the balloons appear as shown in (ii) and (v). After sufficient
159 time for deflection, the balloons restore their initial shape, as shown in (iii) and (vi). The time required for
160 the balloons to fully deflect depends on the experimental conditions. Note that (i–iii) are for the blue balloon
161 to be expanded, and (iv–vi) are for the yellow balloon. These experimental results indicate that balloons
162 can be selectively driven by setting appropriate inflow conditions.

163 **Discussion**

164 Here, we discuss why the desired deformation (defined as (c) in Fig. 6a) is distributed diagonally in Fig.
165 6b, and why there is a difference in time required to restore the initial appearance among the different

166 conditions as shown in Figs. 6c and 6d.

167 Fig. 7 shows a schematic relation between the flow rate of the main flow, Q , and the cross-section ratio of
168 the throttle valve, γ . If the Q increases slightly as

$$173 \quad Q' = Q + \Delta Q, \quad (5)$$

169 the flow rates of outlets 1 and 2 increase (see Fig. 5). The inner pressure of the balloon increases as a
170 function of the throttle valve, and it is proportional to the outlet flow velocity (see Equation 4). Therefore,
171 if the flow rate of the main flow becomes Q' , the inner pressure of both balloons increases, and vice versa.
172 If γ decreases slightly as

$$174 \quad \gamma' = \gamma - \Delta\gamma, \quad (6)$$

175 the inner pressure of both balloons increases, and vice versa. Therefore, if the balloons deform suitably, as
176 shown in Fig. 6a (iii) at the point (Q, γ) in Fig. 7, the close suitable point may be located at $(Q + \Delta Q, \gamma +$
177 $\Delta\gamma)$ and $(Q - \Delta Q, \gamma - \Delta\gamma)$. Then, the relationship between ΔQ and $\Delta\gamma$ should be clarified to understand
178 the reason for the diagonally located experimental result of the desired deformation in Fig. 6b. As we
179 neglect the pressure loss from sudden contraction in Equation 4, the inner pressure of the balloon is
180 expressed as

$$181 \quad \Delta P_{total} = \frac{\rho V_D^2 D^2}{2 d^2} \left(1 - \frac{d^2}{D^2}\right)^2. \quad (4')$$

182 As shown in Equation 4', the pressure is expressed as the product of the square of the flow velocity, V_D ,
183 and the fourth power of the inner diameter ratio at the throttle valve. However, as we use the roller clamp
184 as the throttle valve, Equation 4' can be expressed, using the cross-section ratio γ of the tube instead of the
185 inner diameter ratio, as

$$186 \quad \Delta P_{total} = \frac{\rho V_D^2}{2} \frac{1}{\gamma} (1 - \gamma)^2 = \frac{\rho V_D^2}{2} \left(\frac{1}{\gamma} + \gamma - 2\right). \quad (4'')$$

187 We solved Equation 4'' for $Q (= V_d A)$, γ , and the constant left-hand side, $\Delta P_{total} = 8$ kPa, at which the PV
188 diagram shows a peak (see Fig. 3c). Note that the cross-section, A , was set for $\Delta P_{total} = 8$ kPa when
189 $Q = 13$ mL/s and $\gamma = 0.67$. We superimposed the solved relation between Q and γ onto the desired
190 conditions to obtain the appropriate deformation of balloons ((iii) in Fig. 6a) in Fig. 7b. Even though there
191 is a slight difference, Equation 4'' predicts the diagonal tendency in the graph. When the cross-section ratio

192 is greater than 80%, Equation 4” underestimates the cross-section ratio. The reason may be a pressure loss
193 due to the viscosity and bending of the tube in the actual experimental system. As a result, in an actual
194 situation, the pressure loss increases as the flow rate of the main flow increases, resulting in a lower suitable
195 flow rate. Since the balloons require a threshold pressure of 8 kPa to significantly deform, the inlet flow
196 rate should be sufficiently high or the cross-section ratio should be small enough to obtain this threshold
197 pressure. In other words, when the combination of the flow rate of the main flow and cross-section ratio is
198 not suitable, the inner pressure of the balloon is not high enough to sufficiently inflate the balloon. Therefore,
199 the plots of the desired deformation are located diagonally, as shown in Fig. 6b.

200 When the flow rate of the main flow was high and the balloon inflated ((i) to (ii), and (iv) to (v) in Figs. 6c
201 and 6d), the inner pressure of the balloon increased and then decreased by ΔP_{def} according to the
202 deformation of the balloon, owing to the nonlinear PV diagram shown in Fig. 3c. This means that once the
203 inner pressure exceeds the threshold, it becomes easier for the inflated balloon to inflate, and the deflated
204 balloon to deflate. Therefore, the smaller the ΔP_{def} is, the easier it is for the balloon to deflate ((ii) to (iii),
205 and (v) to (vi) in Figs. 6c and 6d) after the control flow is stopped. The deformability of the balloon depends
206 on ΔP_{def} , which depends on the deformation of the balloon when the control flow is stopped. Moreover,
207 the deformation of the balloon depends on the flow rate of the main flow. Therefore, the time required for
208 the deflation of the balloon increases as the flow rate of the main flow increases. Note that in Fig. 6d, the
209 10.8 mL/s of flow rate of the main flow requires a longer time for deflection compared with Fig. 6c, in
210 which the flow rate of the main flow is 9.5 mL/s.

211

Conclusion

212 To realize the multi-degree-of-freedom motion of a soft robot using embedded fluidic elements, this study
213 proposed a method to selectively inflate a balloon using a fluidic valve, mediated by the Coanda effect,
214 operated by the control flow input. The developed valve is capable of generating a flow difference of
215 approximately 0.25 mL/s between two outlets, and the selective inflation of balloons is realized using a
216 simple configuration when the balloons have peaks in their PV diagram. This shows the possibility of a
217 new driving method for fluid-driven soft robots and that a soft robot with multiple degrees of freedom can
218 be driven only by fluid elements. Because the proposed method suggests that the control strategy may be
219 implemented in the fluid circuit, our future study will focus on the development of a fully fluidically

220 controlled soft robot system.

221 **Declarations**

222 **Funding**

223 Not applicable

224 **Acknowledgements**

225 We would like to thank Editage (www.editage.com) for English language editing.

226 **Author's contributions**

227 KT conceived and designed the experiments; KK developed the experimental system, performed the
228 experiments, and analyzed the data. KK wrote the paper with critical input from KT.

229 **Availability of data and materials**

230 The datasets used and/or analyzed in this manuscript are available from the corresponding author upon
231 reasonable request.

232 **Competing interests**

233 The authors declare that they have no competing interests.

234 **References**

- 235 1. Nishioka Y (2015) Pneumatic soft robot arm. *J Robot Soc Jpn* 33(9):664–667.
236 <https://doi.org/10.7210/jrsj.33.664>
- 237 2. Kim S, Laschi C, Trimmer B (2013) Soft robotics: a bioinspired evolution in robotics. *Trends*

238 Biotechnol 31(5):287–294. <https://doi.org/10.1016/j.tibtech.2013.03.002>

239 3. Shepherd RF, Ilievski F, Choi W, Morin SA, Stokes AA, Mazzeo AD, Chen X, Wang M, Whitesides
240 GM (2011) Multigait soft robot. Proc Natl Acad Sci U S A 108(51):20400–20403.
241 <https://doi.org/10.1073/pnas.1116564108>

242 4. Katzschmann RK, DelPreto J, MacCurdy R, Rus D (2018) Exploration of underwater life with an
243 acoustically controlled soft robotic fish. Sci Robot 3(16). <https://doi.org/10.1126/scirobotics.aar3449>

244 5. Takemura K (2018) Soft robotics using electro-conjugate fluid (in Japanese). Meas Control
245 57(11):775–779

246 6. Cacucciolo V, Shintake J, Kuwajima Y, Maeda S, Floreano D, Shea H (2019) Stretchable pumps for
247 soft machines. Nature 572(7770):516–519. <https://doi.org/10.1038/s41586-019-1479-6>

248 7. Gorissen B, Milana E, Baeyens A, Broeders E, Christiaens J, Collin K, Reynaerts D, De Volder M
249 (2019) Hardware sequencing of inflatable nonlinear actuators for autonomous soft robots. Adv Mater
250 31(3):e1804598. <https://doi.org/10.1002/adma.201804598>

251 8. Zatopa A, Walker S, Menguc Y (2018) Fully soft 3D-printed electroactive fluidic valve for soft
252 hydraulic robots. Soft Robot 5(3):258–271. <https://doi.org/10.1089/soro.2017.0019>

253 9. Wehner M, Truby RL, Fitzgerald DJ, Mosadegh B, Whitesides GM, Lewis JA, Wood RJ (2016) An
254 integrated design and fabrication strategy for entirely soft, autonomous robots. Nature 536(7617):451–
255 455. <https://doi.org/10.1038/nature19100>

- 256 10. Galloway KC, Becker KP, Phillips B, Kirby J, Licht S, Tchernov D, Wood RJ, Gruber DF (2016) Soft
257 robotic grippers for biological sampling on deep reefs. *Soft Robot* 3(1):23–33.
258 <https://doi.org/10.1089/soro.2015.0019>
- 259 11. Polygerinos P, Wang Z, Galloway KC, Wood RJ, Walsh CJ (2015) Soft robotic glove for combined
260 assistance and at-home rehabilitation. *Robot Auton Syst* 73:135–143.
261 <https://doi.org/10.1016/j.robot.2014.08.014>
- 262 12. Tesář V (2004) Fluidic valve for reactor regeneration flow switching. *Chem Eng Res Des* 82(3):398–
263 408. <https://doi.org/10.1205/026387604322870516>
- 264 13. Bettridge M, Smith B, Spal R (2004) Aerodynamic jet vectoring using steady blowing and suction.
265 *Exp Fluids* 40:776–785
- 266 14. White MF (ed.) (2016) *Fluid mechanics*. McGraw-Hill Education, New York

Figures

Figure 1

Overviews of the proposed system to selectively drive balloons with simple fluidics valve mediated with the Coanda effect. **a)** When the control flow 1 is introduced, **b)** when the control flow 2 is introduced.

Figure 2

Overviews of the fluidic switching valve and a throttle valve. **a)** When the control flow 1 is introduced. **b)** When the control flow 2 is introduced. **c)** The Coanda effect observed in the fluidic switching valve. **d)** Cross-section and dimensions of the developed fluidic switching valve. **e)** Actual view of the valve. **f)** An overview of the throttle valve. **g)** Cross-section of the throttle valve. **h)** A model of the throttle valve.

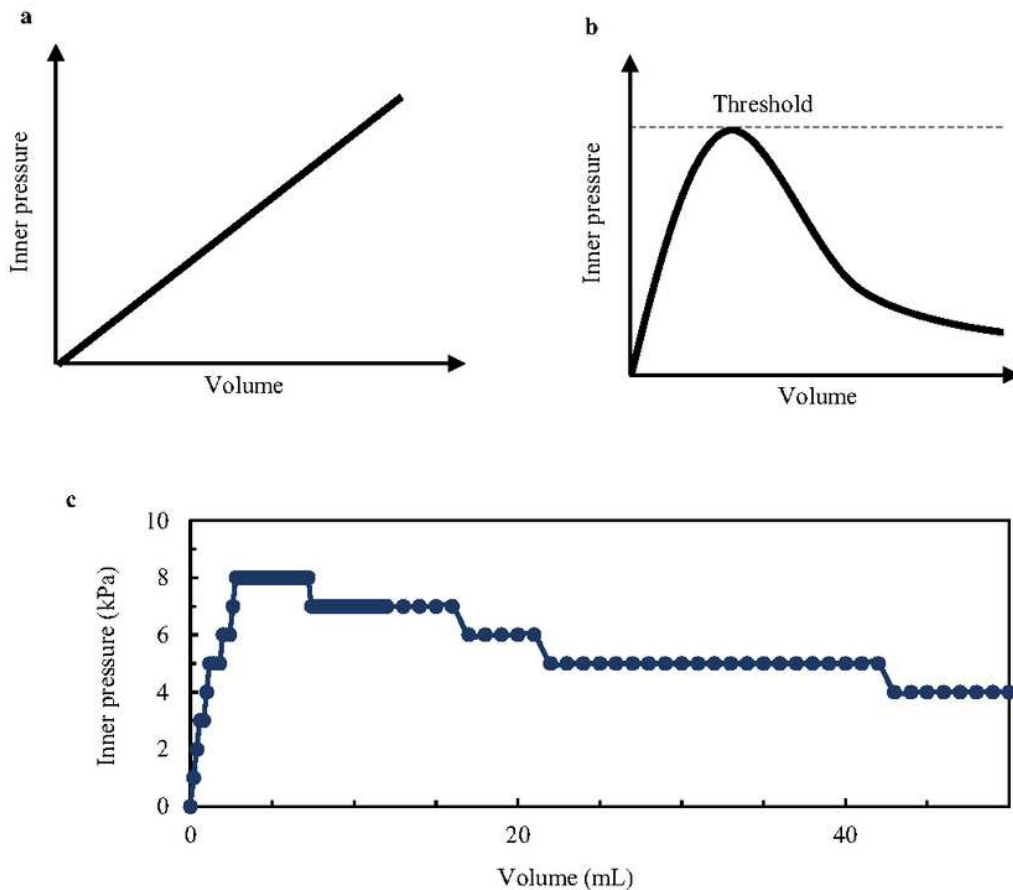


Figure 3

PV diagrams of a balloon. **a)** Linear PV diagram. **b)** Nonlinear PV diagram with a peak. **c)** PV diagrams of a latex balloon employed in this study.

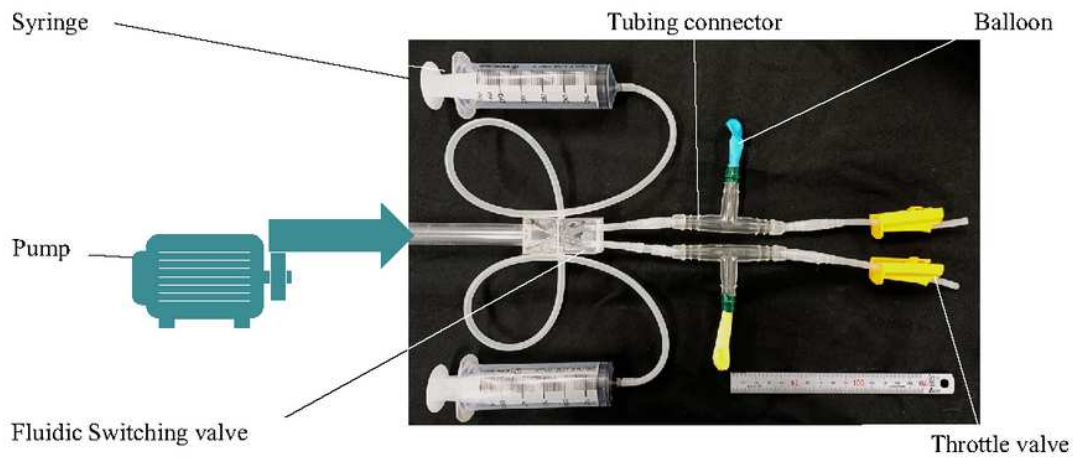


Figure 4

An actual view of the developed system to confirm the feasibility of introducing the fluidic switching valve to soft actuator system.

Figure 5

The experiment for switching characterization. **a)** The set up for the experiment. **b)** the flow rate difference of the outlet 1 against outlet 2.

Figure 6

Balloons deformation experiment. **a)** An evaluation status defined in this experiment. **b)** The summary of the experimental results. **c)** The balloon's deformation under the cross area of 59%, the flow rate of main flow of 9.5 mL/s. (i) $t=0$ s: inflow started. (ii) $t=7.6$ s: the control flow 1 was stopped. (iii) $t=12$ s: the balloon contracted. (iv) $t'=0$ s: inflow started. (v) $t'=7.6$ s: the control flow 2 was stopped. (vi) $t'=14$ s: the balloon contracted. **d)** The balloon's deformation under the cross area of 59%, the flow rate of main flow of 10.8 mL/s. (i) $t=0$ s: inflow started. (ii) $t=7.6$ s: the control flow 1 was stopped. (iii) $t=20$ s: the balloon contracted. (iv) $t'=0$ s: inflow started. (v) $t'=7.6$ s: the control flow 2 was stopped. (vi) $t'=83$ s: the balloon contracted.

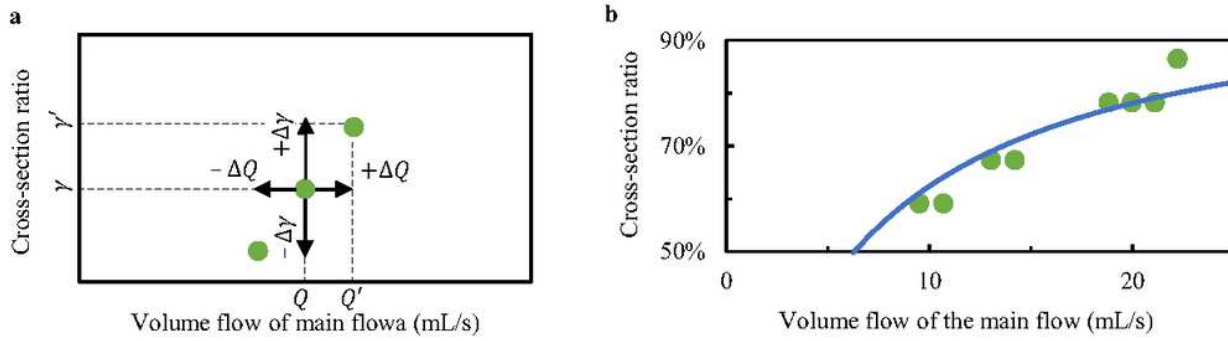


Figure 7

The relation between the main flow rate and the cross-section ratio. a) Schematic relation. b) Comparison between the experimental result and the solution of the pressure loss.